Dynamic dielectric response and electron-energy-loss spectra of individual single-walled BN nanotubes

Vl. A. Margulis*
Department of Physics, N. P. Ogarev Mordovian State University, Saransk 430000, Russia

E. E. Muryumin and E. A. Gaiduk
Department of Chemistry, N. P. Ogarev Mordovian State University, Saransk 430000, Russia
(Received 18 September 2007; published 22 January 2008)

Motivated by the recent electron-energy-loss-spectroscopy (EELS) experiment of Arenal *et al.* [Phys. Rev. Lett. **95**, 127601 (2005)], we investigate the collective π-electronic excitations in individual boron nitride single-walled nanotubes (BN-SWNTs) with a zigzag wrapping. The dynamic dielectric response of such tubes is treated within a self-consistent-field approach using the one-particle states of the π-electron system of the BN-SWNTs derived from a simple two-band tight-binding model. Based on this approach, we obtain explicit analytic expressions for the real and imaginary parts of the frequency- and wave-number-dependent dielectric function of the system, whereby the electron-energy-loss function can easily be calculated. Numerical results for this function are presented for several zigzag BN-SWNTs in order to illustrate the possible electron-energy-loss spectra, and each tube is found to support only one branch of the wave-number-dispersed collective π-plasmon mode for each transferred quantum angular momentum L. In this respect, our results are in good agreement with the experiment, where only one pronounced peak, which can presumably be attributed to the π-plasmon excitations with a small L and a small transferred momentum q, dominates the electron-energy-loss spectra in the range up to 8 eV. The wave-number dispersion of the plasmon modes with different L's is extracted from the calculated spectra of the real part of the dielectric function, and it is shown that the plasmon dispersion curves exhibit a number of unusual characteristics that could be observable in momentum-resolved EELS experiments.

DOI: 10.1103/PhysRevB.77.035425 PACS number(s): 73.22.−f, 73.20.−r, 79.20.Uv

I. INTRODUCTION

In the past decade, there has been steadily expanding interest in the study of boron nitride nanotubes (BN-NTs). They were first predicted theoretically in 1994 (Ref. 1) by analogy with carbon nanotubes (CNTs)[2] and now routinely produced in both multiwalled and single-walled forms by using different techniques (for a brief review of the subject, see Ref. 3). One of the most remarkable properties of BN-NTs is that, unlike CNTs, they are wide-band-gap semiconductors regardless of their diameter, helicity, or the number of the walls of the tube.[4] This feature, combined with excellent mechanical and piezoelectric properties,[5–12] high resistivity to oxidation,[13] and high thermal stability,[14] makes BN-NTs very attractive for innovative applications in various fields of nanoscience and nanotechnology.

In spite of the extensive work that has been done in recent years on the study of BN-NTs, many of their basic physical properties are still poorly understood. In particular, very little is known, at present, about the fundamental characteristics of collective electronic excitations in BN-NTs, which dominate the dynamic dielectric response of the tubes. For further research and application, it would be, therefore, desirable to present theoretical information on the energy of collective excitation modes and their wave-number dispersion in BN-NTs. To the best of our knowledge, no such information is available in the literature. Meanwhile, there have been several experimental studies[15–19] on BN-NTs by means of high-resolution electron-energy-loss spectroscopy (EELS) which directly probes the collective excitations (plasmons in this case). Most of these studies have been performed on multiwalled BN nanotubes (BN-MWNTs) by using non-momentum-resolved EELS measurements.[15–17] This appears to be due to the experimental difficulties in achieving the resolution in momentum in the case of isolated nanotubes. In order to overcome these difficulties, Fuentes *et al.*[18] have used a macroscopic assembly of BN-MWNTs of different diameters and chiralities, which have not, however, been characterized individually. Though the momentum-dependent low-loss spectra measured in Ref. 18 allow the plasmon mode dispersion to be extracted, they provide only an averaged picture of plasmon properties, which makes a detailed comparison with any possible microscopic theory ambiguous.

In more recent work by Arenal *et al.*,[19] EELS has been used to study several individual BN-NTs of known structure, including single-walled BN nanotubes (BN-SWNTs) with diameters ranging from 1.4 to 2.3 nm. However, that study has exploited the non-momentum-resolved spectroscopy method and was aimed to demonstrate that EELS can be used to determine the optical band gap of BN-NTs, rather than to investigate the properties of plasmon excitations in these tubes. This may explain the fact that no detailed discussion has been presented in Ref. 19 regarding the features revealed in the low-loss spectra of BN-NTs. Namely, for three BN-SWNTs examined in Ref. 19, a pronounced broad peak in the spectra at ~6.6–6.9 eV has been observed, which can presumably be attributed to the collective π-plasmon excitations with a small momentum transfer. While the plasmonic nature of the peak was pointed out by Arenal *et al.*,[19] further details,

e.g., about the momentum dependence of the peak, have not been reported in that paper, probably because of the limitations of the experimental method used. In this context, it seems to be an important challenge, on the experimental side, to develop the EELS techniques that can be used to measure the momentum-dependent dielectric response of individual nano-objects, including BN-NTs. On the theoretical side, it is now imperative to develop a theory of collective plasmon excitations in BN-NTs, which would allow specific quantitative predictions to be made regarding the characteristics of the plasmon modes. The first step in this direction has already been made by Marinopoulos *et al.*[20] and Guo and Lin,[21] who performed first-principles density-functional-theory calculations of the electron-energy-loss spectra for several representative BN-SWNTs of very small diameters. They revealed the pronounced peaks in the spectra, some of which can be ascribed to the low-frequency π plasmons, whereas the other—to the high-frequency collective oscillations of the combined $\pi+\sigma$ electron system, commonly known as $\pi+\sigma$ plasmons. However, the theoretical modeling carried out in Refs. 20 and 21 was restricted to the optical limit, i.e., to the zero momentum transfer, and, as a consequence, no results on the plasmon dispersion in BN-NTs have been obtained in those papers.

In this paper, we report on our theoretical investigation of the dynamic-dielectric-response properties of individual BN-SWNTs. Our main goal here is to present a systematic study of the collective plasmon excitations and electron-energy-loss spectra of these nanotubes. We restrict our attention to the collective plasmon modes associated with π electrons alone, disregarding the $\pi+\sigma$-plasmon branches of the collective excitations. The π plasmons correspond to the experimentally identified peaks in the low-energy region (<15 eV) of the loss spectra, whereas the $\pi+\sigma$ plasmons exhibit themselves as the peaks located at higher energies.[19] Our treatment of the collective π-electronic excitations follows the line of the theory of plasmons in solids, originally developed by Ehrenreich and Cohen[22] on the basis of a self-consistent-field approach. More recently, this approach has successfully been used by Lin *et al.*[23] to describe plasmon excitations in isolated CNTs (see also a recent paper by Perez and Que,[24] and references therein). The key quantity that determines the properties of the plasmons is the frequency- and wave-number-dependent dielectric function $\varepsilon(\omega,q)$ of the system. Although this quantity in the limit $q\rightarrow 0$ has already been calculated for BN-SWNTs by using different methods,[20,21,25] to the best of our knowledge, the corresponding full dynamic-dielectric-response function $\varepsilon(\omega,q)$ has not yet been addressed to. To calculate the $\varepsilon(\omega,q)$, the electronic structure of BN-SWNTs needs to be known, which we derive using a simple tight-binding model that describes the energy bands of BN-SWNTs in terms of two semiempirical parameters.

An outline of the remainder of this paper is as follows. In Sec. II we develop the constitutive equations for the theory of the dynamic dielectric response of individual BN-SWNTs. Then, in Sec. III we present the results for the electron-energy-loss spectra of several representative BN-SWNTs with a zigzag structure, obtained from our numerical calculations, and discuss the trends and the characteristic behaviors they illustrate. The π-plasmon dispersion curves, extracted from the spectra of the real part of $\varepsilon(\omega,q)$, are also presented in Sec. III. To the extent possible, we make direct comparisons with the experiments of Refs. 18 and 19. Finally, in Sec. IV we briefly summarize our conclusions.

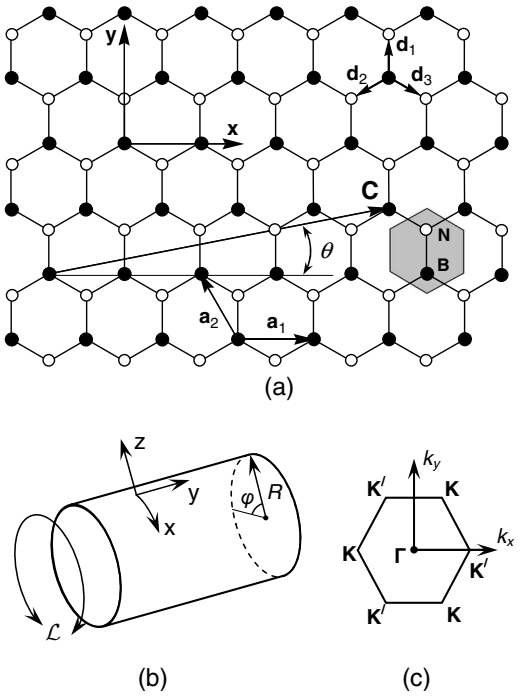

FIG. 1. Lattice structure of a two-dimensional BN sheet (a), geometrical structure of a BN-SWNT (b), and the first Brillouin zone of the BN sheet (c). The shaded hexagon represents a unit cell of the BN sheet. Two primitive translation vectors of lattice structure are denoted by $\mathbf{a}_1$ and $\mathbf{a}_2$. Three vectors directed from a B site to nearest-neighboring N sites are given by $\mathbf{d}_i(i=1,2,3)$. A BN-SWNT is specified by a chiral vector $\mathbf{C}$ indicating the direction in which the BN sheet is rolled up to form a nanotube. For the zigzag BN-SWNTs under consideration we choose the coordinate system xyz with the x axis along the circumference direction and the y axis along the tube axis. For other notations, see the text.

II. BASIC THEORY

It seems to be appropriate to separate the discussion of the present section into two parts. First, we consider the π-electronic band structure of BN-SWNTs within a tight-binding approximation (Sec. II A). Then, we calculate the dielectric response of an individual BN-SWNT by using a self-consistent-field approach (Sec. II B).

A. Electronic structure of boron nitride single-walled nanotubes

We start with recalling the geometrical structure of BN-SWNTs. An individual BN-SWNT can be viewed as being constructed from a strip of a BN sheet by rolling it up to form a cylinder, as shown in Fig. 1. Although in practice BN-SWNTs are certainly not produced in that way, the idea to treat them as a wrapping BN sheet is very appealing from

the theoretical standpoint, since it allows their electronic band structure to be rationalized (see further below).

The wrapped structure of the nanotubes can be specified in terms of a pair of two integers (l_1,l_2), which uniquely determine the rolling-up or circumference vector $\mathbf{C}$ as follows:

$$\mathbf{C} = l_1\mathbf{a}_1 + l_2\mathbf{a}_2, \tag{1}$$

where $\mathbf{a}_1$ and $\mathbf{a}_2$ are the primitive lattice translation vectors of a two-dimensional hexagonal BN network, making an angle of 120° [see Fig. 1(a)]. Choosing the Cartesian coordinate axes x and y in such a way that the x axis is parallel to the vector $\mathbf{a}_1$, we have

$$\mathbf{a}_1 = a_0(1,0), \quad \mathbf{a}_2 = a_0\left(-\tfrac{1}{2},\tfrac{\sqrt{3}}{2}\right), \tag{2}$$

where the lattice constant $a_0=|\mathbf{a}_1|=|\mathbf{a}_2|$ is equal to $\sqrt{3}$ multiplied by the B-N bond length $d=1.45$ Å. The two main geometrical parameters of the nanotube (l_1,l_2)—namely, its radius R and the chiral angle θ—are then expressed as follows:

$$R = \frac{a_0}{2\pi}\sqrt{l_1^2 + l_2^2 - l_1 l_2}, \tag{3}$$

$$\theta = \tan^{-1}\left(\frac{\sqrt{3}l_2}{2l_1 - l_2}\right). \tag{4}$$

Just like single-walled CNTs,[2] BN-SWNTs are subdivided into two groups, depending on their symmetry, namely, chiral and achiral nanotubes. The two special classes of the latter are the so-called zigzag $(l,0)$ nanotubes and the armchair (l,l) ones. An interesting feature of BN-SWNTs is that, unlike CNTs, they "prefer" to have a zigzag wrapping during their growth in current synthesis processes.[26,27] Therefore, in what follows we restrict our attention to the case of the zigzag BN-SWNTs.

To calculate the electronic band structure of these nanotubes, we adopt a simple physical scheme based on the nearest-neighboring tight-binding (TB) model and the zone-folding method.[2] This approach has previously been successfully used to model the electronic structure of single-walled CNTs.[2] Although the approach lacks the accuracy that more sophisticated *ab initio* methods are able to provide, especially for the thinnest nanotubes, the great advantage of the approach is that it allows the electronic structure of the nanotubes to be derived in a closed analytical form. Provided the proper choice of the parameters entering the TB model is made, it yields a reasonably good description of the basic properties of the electronic structure of the CNTs, not being, thereby, as much computationally expansive as more sophisticated models. This provides a motivation for the similar treatment of the band structure of BN-SWNTs, which, though rather trivial, has, to our knowledge, not yet been reported in the literature.[28]

We focus our attention on the two principle bands (valence and conduction) formed by π orbitals, since it is just these π bands that basically determine the low-energy physics of BN-SWNTs (below ~15 eV). In the case of a BN sheet, the edges of the corresponding π bands are located at the K and K' points of the two-dimensional Brillouin zone of the sheet [see Fig. 1(c)]. Without loss of generality, we choose two inequivalent K and K' points, whose wave vectors are given by

$$\mathbf{K} = \frac{2\pi}{a_0}\left(\frac{1}{3},\frac{1}{\sqrt{3}}\right), \quad \mathbf{K}' = \frac{2\pi}{a_0}\left(\frac{2}{3},0\right). \tag{5}$$

In the TB approximation, where only nearest-neighbor interactions are retained, the Hamiltonian for the π electrons of the BN sheet is expressed by a 4×4 matrix, containing two independent 2×2 blocks, namely, the upper left and the lower right, corresponding to the two above-mentioned $\mathbf{K}$ and $\mathbf{K}'$ points. The Hamiltonian matrix H_{2D} associated with the $\mathbf{K}$ point is given by

$$H_{2D} = \begin{pmatrix} \Delta & h(\mathbf{k}) \\ h^*(\mathbf{k}) & -\Delta \end{pmatrix} \tag{6}$$

with

$$h(\mathbf{k}) = -t_0\sum_{i=1}^{3}\exp(i\mathbf{k}\mathbf{d}_i), \tag{7}$$

where $\mathbf{k}(k_x,k_y)$ is the two-dimensional electron wave vector, measured relative to the $\mathbf{K}$ point, and the vectors $\mathbf{d}_i(i=1,2,3)$, which connect three nearest-neighboring N atoms with a B atom [see Fig. 1(a)], are defined as

$$\mathbf{d}_1 = a_0\left(0,\tfrac{1}{\sqrt{3}}\right), \quad \mathbf{d}_2 = a_0\left(-\tfrac{1}{2},-\tfrac{1}{2\sqrt{3}}\right),$$

$$\mathbf{d}_3 = a_0\left(\tfrac{1}{2},-\tfrac{1}{2\sqrt{3}}\right), \tag{8}$$

so that $h(\mathbf{k})$ can be expressed as

$$h(\mathbf{k}) = -t_0\left[\exp\left(\frac{ik_y a_0}{\sqrt{3}}\right) + 2\exp\left(-\frac{ik_y a_0}{2\sqrt{3}}\right)\cos\left(\frac{k_x a_0}{2}\right)\right]. \tag{9}$$

We have parametrized the Hamiltonian H_{2D} of Eq. (6) by the difference 2Δ of energies of π electrons localized on the B and N sites and by the transfer integral t_0 between π orbitals of nearest-neighboring B and N atoms.

By solving the Schrödinger equation with the above-mentioned Hamiltonian H_{2D}, the π-electron-energy dispersion for the valence (v) and conduction (c) bands of the BN sheet can readily be obtained. The π bands of a BN-SWNT can then be deduced from those of the BN sheet by using the zone-folding method.[2] In this method, the wrapping of a BN sheet into a BN-SWNT imposes restrictions on the available values of the electron wave vector in the direction perpendicular to the nanotube axis. For the zigzag $(l,0)$ BN-SWNTs we are concerned with here, the x component of the electron wave vector $\mathbf{k}$ is quantized into the following discrete values:

$$k_x = \frac{2\pi m}{la_0}, \quad m = 0, \pm1, \pm2, \ldots, \pm(l-1), \tag{10}$$

due to the periodic boundary condition in the circumference direction of the nanotube. As a result, the π bands of the BN sheet are split into a set of one-dimensional energy subbands, which are determined by the equation

$$E_{smk} = \pm \sqrt{\Delta^2 + t_0^2[1 + 4\nu_m^2 + 4\nu_m \cos(kd_0/2)]} \quad (11)$$

with

$$\nu_m = \cos\left(\frac{\pi m}{l}\right), \quad d_0 = \sqrt{3}a_0 = 3d, \quad (12)$$

where $s(=c,v)$ is the band index and k is the one-dimensional wave vector along the tube axis. We consider an infinitely long nanotube, so that all the inequivalent values of k are contained within the one-dimensional Brillouin zone of the nanotube with a center at the Γ point [see Fig. 1(c)], i.e., $k \in [-k_{BZ}, k_{BZ}]$, where $k_{BZ} = \pi/d_0$ for a zigzag nanotube. The upper (lower) sign on the right-hand side of Eq. (11), as well as of the forthcoming equation, refers to the $c(v)$ band.

The eigenstates, corresponding to the energy eigenvalues E_{smk} of Eq. (11), are given by the following pseudospinor:

$$\mathbf{C}_{smk} = \begin{pmatrix} C_{smk}^{(1)} \\ C_{smk}^{(2)} \end{pmatrix} = \frac{1}{\sqrt{2E_{cmk}}} \begin{pmatrix} \dfrac{h_{mk}}{\sqrt{E_{cmk} \mp \Delta}} \\ \pm\sqrt{E_{cmk} \mp \Delta} \end{pmatrix}, \quad (13)$$

whose two components $C_{smk}^{(1)}$ and $C_{smk}^{(2)}$ correspond to the wave function's amplitudes at the sites of the two sublattices occupied by B and N atoms, respectively. Here the quantity h_{mk}, as derived from Eq. (9) using Eqs. (10) and (12), is given by

$$h_{mk} = -t_0[\exp(ikd) + 2\nu_m \exp(-ikd/2)]. \quad (14)$$

Within the TB approximation, the periodic part of the Bloch function for the π bands of a BN-SWNT, which we will need further in this paper, can be written as follows:

$$u_{smk}(\mathbf{r}) = \sum_{j=1,2} C_{smk}^{(j)} U_{\mathbf{k}}^{(j)}(\mathbf{r}), \quad (15)$$

where each of the periodic functions $U_{\mathbf{k}}^{(j)}(\mathbf{r})(j=1,2)$ is further expressed by a linear combination of atomic $2p_z$ orbitals $\phi(\mathbf{r}-\mathbf{R}_n-\boldsymbol{\tau}_j)(n=1,2,\ldots,N)$ as follows:

$$U_{\mathbf{k}}^{(j)}(\mathbf{r}) = \frac{1}{\sqrt{N}} \sum_n e^{-i\mathbf{k}(\mathbf{r}-\mathbf{R}_n-\boldsymbol{\tau}_j)} \phi(\mathbf{r} - \mathbf{R}_n - \boldsymbol{\tau}_j). \quad (16)$$

Here $\mathbf{R}_n$ stands for the position vector of the nth unit cell, $\boldsymbol{\tau}_j$ denotes the vector connecting the two atoms within a unit cell, i.e.,

$$\boldsymbol{\tau}_j = \delta_{j2}\mathbf{d}_1 \quad (17)$$

(δ_{j2} is the Kronecker delta symbol), and N is the total number of the sites occupied by B and N atoms, which is given by

$$N = \frac{4A\mathcal{L}}{\sqrt{3}a_0^2}, \quad (18)$$

where A is the normalized length of the nanotube and $\mathcal{L}$ its circumference length.

We conclude the discussion of the zone-folding-derived π-band structure of the zigzag BN-SWNTs by noticing that the corresponding electronic states are doubly degenerate due to the presence of the states associated with the $\mathbf{K}'$ point of the original Brillouin zone of a BN sheet. The energy subbands associated with this point are exactly the same as those in Eq. (11), and this is in full agreement with the time-reversal-symmetry requirement.[29] In addition, there is certainly a trivial double degeneracy of the states due to the spin degree of freedom. Both the above-mentioned degeneracies will be taken into account further below in calculating the dielectric function of a BN-SWNT.

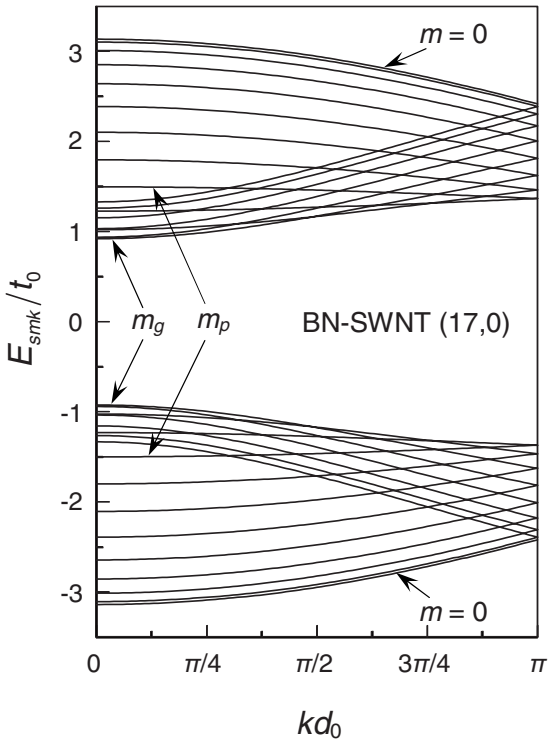

FIG. 2. Plot of the π-electronic energy subbands E_{smk} for the BN-SWNT (17,0), as obtained within the tight-binding model. One pair of arrows indicates the highest valence and lowest conduction subbands corresponding to the azimuthal quantum number $m=m_g$. The other pair of arrows points out the pair of subbands, specified by the quantum number $m=m_p$, which play a key role in the formation of the interband $L=0$ plasmon mode in the nanotube under consideration. The above-mentioned quantum numbers m_g and m_p are equal to 9 and 8, respectively, in the case of the BN-SWNT (17,0). For details, see the text.

In Fig. 2 we show the normalized π-electron-energy-subband dispersions plotted as E_{msk}/t_0 versus kd_0 for a zigzag (17,0) BN-SWNT of about 1.35 nm in diameter. For such a nanotube, as well as for other large diameter BN-SWNTs, the finite-tube-curvature effects, including σ-π hybridization, are expected to play a minor role,[21] so that the model proposed above seems to be appropriate for those nanotubes. The band structure depicted in Fig. 2 has been calculated using the following values of the parameters Δ and t_0 entering Eq. (11): $\Delta=2.2$ eV and $t_0=2.4$ eV. The former value has also been adopted in our previous paper,[25] which was focused on the optical properties of the zigzag BN-SWNTs and where it was shown that rather good agreement between the optical absorption experiment[30] and the theoretical calculation can be achieved with that value of the

parameter. Nevertheless, it should be stressed that we do not claim that the above-mentioned values of Δ and t_0 are exactly appropriate to the nanotubes under consideration. The point is that both the parameters are adjustable ones within the TB model and, as such, should be chosen to give the best fit to experimentally derived band structure of BN-SWNTs. However, unlike CNTs, for which the only adjustable parameter is the nearest-neighbor hopping integral t_0, in the case of BN-SWNTs we should handle the two parameters Δ and t_0 to fit a single number, namely, the value of the band-gap energy Δ_g at $k=0$, which, according to Eq. (11), is expressed as

$$\Delta_g = 2\sqrt{\Delta^2 + t_0^2(1+2\nu_{m_g})^2}, \tag{19}$$

the integer m_g being equal to

$$m_g = \left[\frac{l}{2}+1\right], \tag{20}$$

where the square brackets stand for the integral part of the number they contain in. It is evident that in such a case the fitting procedure will scarcely be able to give an unambiguous result unless we know even one of the parameters Δ or t_0 beforehand. The parameter Δ, defined as half the difference of energies of π electrons localized on B and N atoms, is particularly hard to be estimated (or measured) independently with high accuracy, and we are not aware of any relevant experimental data. As to the parameter t_0, there are also no experimental data or first-principles calculations available at present, which would allow us to make a proper choice of its value appropriate for BN-SWNTs. For the structurally similar CNTs, reported values of t_0 range from 2.4 to 3 eV. Thus, the value of $t_0=2.4$ eV, we have taken as a representative one for BN-SWNTs, though reasonable, is certainly rather arbitrary and can be varied at will, if it is necessary to get the best fit to experimental data.

There is one more point that makes the above-mentioned fitting procedure ambiguous. Namely, the very band-gap energy for BN-SWNTs is still not well known from experiment. The value of Δ_g, close to 4.5 eV, is extracted from the optical absorption spectrum measured by Lauret *et al.*[30] for an assembly of BN-SWNTs with an average diameter of about 1.4 nm, whereas evidence for a band-gap value of 5.8 ± 0.2 eV was found in a recent EELS experiment by Arenal *et al.*,[19] performed on individual BN-SWNTs with diameters ranging from 1.4 to 2.3 nm. A scanning tunneling spectroscopy study, carried out by Wang *et al.*[31] on an array of vertically aligned BN-NTs, yielded the band-gap values varied in the range 4.4–4.9 eV. Although this result is in reasonable agreement both with the optical measurement[30] and the theoretical calculations[21,32–35] based on the density-functional theory, the discrepancy between the Δ_g values, reported by different authors, suggests that further systematic experimental work is still necessary in order to obtain reliable data regarding the band-gap energy of BN-SWNTs.

In the light of the above discussion, it is quite clear that the plot of the π bands in Fig. 2 can serve only for illustrative purposes, demonstrating the most important qualitative features of the typical band structure of the zigzag BN-SWNTs. As is seen from that figure, the (empty) conduction and the (filled) valence energy subbands, classified by the azimuthal quantum number m, are mirror symmetric with respect to the Fermi level $E_F=0$. For the BN-SWNTs $(l,0)$ with l being an odd number, the sequence of the energy subbands of the c band at $k=0$ is as follows. The highest subband corresponds to $m=0$ and is characterized by "anomalous" dispersion (the term is borrowed from optics, where it is used in another context) in the sense that E_{cok} decreases monotonically as the wave number k increases. The next lower subbands, which are doubly degenerate in m and also characterized by anomalous dispersion, correspond (from top to bottom in sequential order) to $m=\pm1,\pm2,\ldots,\pm(m_g-1)$, where m_g is defined by Eq. (20). The crossover to normal dispersion of the energy subbands, for which E_{cmk} is a monotone increasing function of k, occurs at $m=\pm m_g$ with m_g being the index of the lowest subband of the c band. The next subbands, which lie higher than the $\pm m_g$ subband and also disperse upward, correspond (again in sequential order, but now from bottom to top) to $m=\pm(m_g+1),\pm(m_g+2),\ldots,\pm(l-1)$. If l is an even number, then the sequence of the subbands remains the same as indicated above, except for the appearance of a doubly degenerate flat (dispersionless) subband specified by the index $m=\pm l/2$. Note that the π-electronic states of the BN-SWNTs do not possess any special symmetry at an arbitrary k point of the nanotube Brillouin zone and therefore the energy subbands with different m can cross without interacting throughout the Brillouin zone, except for the Γ point. It is these multiple crosses that we can observe in Fig. 2.

We will show in Sec. III that, like the case of CNTs,[23,36] the basic feature of the band structure of the BN-SWNTs, relevant to the interband collective electronic excitations in these nanotubes, is just the presence of the energy subbands that disperse upward and downward in both the v and c bands.

B. Dielectric function of a boron nutride single-walled nanotube

We now focus on the dynamic dielectric function of individual zigzag BN-SWNTs, which determines their electron-energy-loss spectrum. As has been mentioned in Sec. I, the EELS studies of BN-NTs reported in Refs. 15–19 motivate us to calculate the spectrum observed in such a type of experiments. To carry out the calculation, we employ the self-consistent-field approach developed by Ehrenreich and Cohen[22] a long time ago. The limitations of the approach will become clear as we develop the theory and they will be under discussion in the end of the section.

A π-electronic system of a BN-SWNT is assumed to be subjected to an external time-dependent electric perturbation of frequency ω, which creates an induced potential through charge redistribution. The latter in turn occurs due to the Coulomb interaction of the π electrons, which is described by the potential $V(\mathbf{r}-\mathbf{r}')=e^2/|\mathbf{r}-\mathbf{r}'|$. Because of cylindrical symmetry of the nanotube, the Fourier component $V_L(q)$ of this potential depends not only on the momentum transfer q along the nanotube axis, but also on the transferred angular momentum $L=0,\pm1,\pm2,\ldots$ in the circumference direction

of the nanotube, and so does the dielectric function $\varepsilon_L(\omega,q)$, which describes the dynamic screening of the external field. Writing $|\mathbf{r}-\mathbf{r}'|$ in cylindrical coordinates (R,φ,y) [see Fig. 1(c)], one obtains the Fourier-series expansion of the Coulomb potential

$$V(\mathbf{r}-\mathbf{r}') = \sum_{L=-\infty}^{\infty} \sum_{q} V_L(q) e^{iL(\varphi-\varphi')} e^{iq(y-y')} \tag{21}$$

with

$$V_L(q) = \frac{2e^2}{A} F_L(|q|R) = \frac{2e^2}{A} I_L(|q|R) K_L(|q|R), \tag{22}$$

where $I_L(|q|R)$ and $K_L(|q|R)$ are the Lth-order modified Bessel functions of the first and second kinds, respectively.

The well-known formula for the longitudinal dielectric function of solids, obtained by Ehrenreich and Cohen,[22] can be readily adapted to describe the dielectric response of the nanotubes we are interested in here, and the result is

$$\varepsilon_L(\omega,q) = \varepsilon_b - V_L(q) \sum_{s,s'} \sum_{m=-(l-1)}^{l-1} \sum_{k} |\langle smk|s',m+L,k+q\rangle|^2 \times \frac{f_0(E_{s',m+L,k+q}) - f_0(E_{smk})}{E_{s',m+L,k+q} - E_{smk} - \hbar\omega - i\hbar\Gamma}, \tag{23}$$

where we have introduced a background dielectric constant ε_b to represent the contribution to the response due to all high-frequency excitations other than the π-electronic ones. In the equation given above, $f_0(E)$ is the Fermi-Dirac distribution function, Γ is a phenomenological level broadening parameter, and the abbreviation

$$\langle smk|s',m+L,k+q\rangle \equiv \int u^*_{smk}(\mathbf{r}) u_{s',m+L,k+q}(\mathbf{r}) d\mathbf{r} \tag{24}$$

has been used, in which the integration extends over a unit cell.

To calculate the integral of Eq. (24) by substituting the function of Eq. (15) for the Bloch amplitude $u_{smk}(\mathbf{r})$, one needs to know the atomic wave function $\phi(\mathbf{r}-\mathbf{R}_n-\boldsymbol{\tau}_j)$ entering Eq. (16). An explicit form of this function cannot be certainly derived analytically, so that the use of approximations in carrying out the integration is unavoidable. Two possible means suggest themselves to perform such an integration. The first, which we will rely on further, is based on the assumption that the periodic part $U^{(j)}_{\mathbf{k}}(\mathbf{r})$ of the Bloch amplitude in Eq. (15) can be taken at $\mathbf{k}=\mathbf{K}$, i.e., at the band edge. Assuming the overlap between the atomic wave functions on the nearest-neighboring sites to be negligibly small, we can easily perform the integration even without knowing the explicit form of $\phi(\mathbf{r}-\mathbf{R}_n-\boldsymbol{\tau}_j)$. After some algebra, we then find

$$|\langle smk|s',m+L,k+q\rangle|^2 = \frac{1}{2}\left[1 \pm \frac{\mathrm{H}_{mL}(k,q)+\Delta^2}{E_{cmk}E_{c,m+L,k+q}}\right], \tag{25}$$

where we have defined $\mathrm{H}_{mL}(k,q)$ as

$$\mathrm{H}_{mL}(k,q) = \tfrac{1}{2}(h^*_{mk}h_{m+L,k+q} + h_{mk}h^*_{m+L,k+q}). \tag{26}$$

The upper (+) and the lower (−) signs on the right-hand side of Eq. (25) correspond to $s=s'=c(v)$ and $s=c(v)$, $s'=v(c)$, respectively.

Alternatively, the integration in Eq. (24) could be carried out analytically if we used approximate atomic wave functions in the form suggested by Slater.[37] It is just this way that, following Shung,[38] has been chosen in Ref. 24, where the collective electronic excitations in CNTs were studied. Within this approach, a q-dependent prefactor of the form similar to that derived in Refs. 24 and 38 should appear on the right-hand side of Eq. (25). This prefactor is very close to 1 for small q values in the sense of $qa_B \ll Z$, where a_B is the Bohr radius and Z is an effective atomic number equal, according to the Slater prescriptions,[37] to 2.6 and 1.9 for B and N atoms, respectively. Hence, the correction due to this prefactor has negligible influence on the dielectric function as long as q is not too much close to the edge of the nanotube Brillouin zone. Since such large values of q will not be treated further, we may safely ignore the above-mentioned correction. Besides, we would like to emphasize that such a correction by itself is not particularly reliable because of the essentially approximate character of the Slater wave functions, and this is an additional argument for not to treat it at all, at least at the present stage.

Noting that the band-gap energy Δ_g of BN-SWNTs is much larger than the thermal energy k_BT (k_B is the Boltzmann constant) even at room temperature ($k_BT \simeq 26$ meV), we can take $f_0(E_{smk})$ in Eq. (23) to be equal to 1(0) for the $v(c)$ band. Further we proceed as follows. After substituting Eqs. (11), (22), and (25) into Eq. (23), we convert the sum over k into the integral over the same variable by using the prescription

$$\sum_{k} \to 4\frac{A}{2\pi}\int_{-k_{\mathrm{BZ}}}^{k_{\mathrm{BZ}}} dk, \tag{27}$$

where the prefactor 4 originates from the summation over two spin states for each of the two valleys at the $\mathbf{K}$ and $\mathbf{K}'$ points, respectively.

Since $\varepsilon_L(\omega,q)$ in Eq. (23) is complex, it needs to be separated into real and imaginary parts. To represent both of them in a convenient form, we express all the relevant energy quantities and the wave numbers in units of t_0 and k_{BZ}, respectively, introducing the following notations:

$$x = \frac{k}{k_{\mathrm{BZ}}}, \quad u = \frac{q}{k_{\mathrm{BZ}}}, \quad z = \frac{\hbar\omega}{t_0},$$

$$\gamma = \frac{\hbar\Gamma}{t_0}, \quad \delta = \frac{\Delta}{t_0}. \tag{28}$$

Our analytical result for the dielectric function can then be summarized as follows:

$$\mathrm{Re}\,\varepsilon_L(\omega,q) = \mathrm{Re}\,\varepsilon_L(z,u) = \varepsilon_b + \frac{2e^2k_{\mathrm{BZ}}}{\pi t_0}F_L\left(\frac{lu}{2\sqrt{3}}\right) \times \sum_{m=-(l-1)}^{l-1}\int_{-1}^{1} W_{mL}(u,\gamma,\delta|x) \times [P_{mL}(z,u|x)Q_{mL}(z,u,\gamma|x) + P_{mL}(-z,u|x)Q_{mL}(-z,u,\gamma|x)]dx, \quad (29)$$

$$\mathrm{Im}\,\varepsilon_L(\omega,q) = \mathrm{Im}\,\varepsilon_L(z,u) = \gamma\frac{2e^2k_{\mathrm{BZ}}}{\pi t_0}F_L\left(\frac{lu}{2\sqrt{3}}\right)\sum_{m=-(l-1)}^{l-1}\int_{-1}^{1} W_{mL}(u,\gamma,\delta|x) \times [Q_{mL}(z,u,\gamma|x) - Q_{mL}(-z,u,\gamma|x)]dx \quad (30)$$

with

$$W_{mL}(u,\gamma,\delta|x) = 1 - \frac{\eta_{mL}(u,x)+\delta^2}{\xi_m(x)\xi_{m+L}(x+u)}, \quad (31)$$

$$P_{mL}(z,u|x) = \xi_m(x) + \xi_{m+L}(x+u) - z, \quad (32)$$

$$Q_{mL}(z,u,\gamma|x) = [P_{mL}^2(z,u|x) + \gamma^2]^{-1}, \quad (33)$$

where

$$\xi_m(x) = [1+\delta^2+4\nu_m^2+4\nu_m\cos(\pi x/2)]^{1/2}, \quad (34)$$

$$\eta_{mL}(u,x) = \cos\left(\frac{\pi u}{3}\right) + 4\nu_m\nu_{m+L}\cos\left(\frac{\pi u}{6}\right) + 2\nu_m\cos\left[\frac{\pi}{2}\left(x+\frac{2u}{3}\right)\right] + 2\nu_{m+L}\cos\left[\frac{\pi}{2}\left(x+\frac{u}{3}\right)\right]. \quad (35)$$

Although the above expressions involve only elementary functions, neither the integral nor the sum in Eqs. (29) and (30) can be evaluated analytically. However, the important computational advantage of Eqs. (29) and (30) is that they can readily be programed to enable numerical results to be obtained, and these are shown in Sec. III.

We close the present section by pointing out that, as in the original formulation proposed by Ehrenreich and Cohen,[22] local-field effects are not included in the theory developed above. Meanwhile, the system under consideration—namely, an individual BN-SWNT—can be viewed as a one-dimensional crystal with the translation periodicity along the direction of the tube axis. It is well known[39,40] that for crystalline solids the dielectric response to an external perturbation of a small wave vector $\mathbf{q}$ involves not only the macroscopic component of the charge density fluctuation at the same $\mathbf{q}$, but also the microscopic corrections of large wave vector $\mathbf{q}+\mathbf{G}$ ($\mathbf{G}$ is a reciprocal lattice vector) due to local-field fluctuations on the atomic scale. Formally, these local-field corrections are associated with the off-diagonal elements of a microscopic dielectric matrix $\varepsilon_{\mathbf{GG}'}(\omega,\mathbf{q})$ of infinite dimension, defined as[39]

$$\varepsilon_{\mathbf{GG}'}(\omega,\mathbf{q}) = \varepsilon(\omega,\mathbf{q}+\mathbf{G},\mathbf{q}+\mathbf{G}'). \quad (36)$$

The above-mentioned nondiagonal elements contribute to the macroscopic dielectric function $\varepsilon_{\mathrm{mac}}(\omega,\mathbf{q})$, which is determined as

$$\varepsilon_{\mathrm{mac}}(\omega,\mathbf{q}) = [(\varepsilon^{-1})_{\mathbf{GG}'}]^{-1}|_{\mathbf{G}=\mathbf{G}'=0}. \quad (37)$$

The necessity of matrix inversion makes the evaluation of $\varepsilon_{\mathrm{mac}}(\omega,\mathbf{q})$ using Eq. (37) rather complicated. Generally, the problem can be solved only numerically after a truncation of the infinite dimensional matrix of Eq. (36) up to a submatrix of a finite dimension. Such calculations using submatrices of different dimensions have recently been performed by Perez and Que[24] for individual CNTs. The results they obtained show that the local-field effects are negligible at least for nanotubes of sufficiently large diameters (more than 1.4 nm). We believe that it is reasonable to speculate on the validity of this conclusion for BN-SWNTs as well.

III. ELECTRON-ENERGY-LOSS SPECTRA AND DISPERSION OF PLASMONS

In this section we first present the results of our numerical study of Eqs. (29) and (30) for, respectively, the real and the imaginary parts of the dielectric function $\varepsilon_L(\omega,q)$. Figure 3 shows $\mathrm{Re}\,\varepsilon_L(\omega,q)$ and $\mathrm{Im}\,\varepsilon_L(\omega,q)$ as functions of the dimensionless frequency $\hbar\omega/t_0$ for the BN-SWNT (17,0). The plots depicted in that figure are obtained using the same values of the parameters Δ and t_0 as indicated is Sec. II A with the addition of $\hbar\Gamma=2.4$ meV and $\varepsilon_b=2.5$. It should be stressed that neither of the two last parameters is extracted directly from experiment and neither of them is taken to be adjusted to some experiment. Nevertheless, the above value of the dielectric constant ε_b, describing the screening due to all excitations outside the π bands, appears to be realistic for the nanotubes under consideration (see Ref. 41, where the full static dielectric constant of BN-SWNTs has been calculated using a finite-electric-field method). For L, two different values $L=0,1$ have been taken in order to illustrate the effect of the transferred angular momentum on the calculated spectra of the dielectric function at a fixed small, but finite value of the wave number q (equal to $0.2k_{\mathrm{BZ}}$ in this case). We would like to emphasize that the results in Fig. 3 are typical of those we have obtained for other zigzag BN-SWNTs $(l,0)$ (with $l>17$) we have examined.

As is obvious from Eq. (23), if $L=0$, then the main single-particle excitation processes that contribute to the dielectric function are interband electron transitions between the pairs of energy subbands with one and the same azimuthal quantum number m. The probability of such transitions (which, for brevity, will further be designated by $v_m \to c_m$) is extremely large near the subband edges at the $k=0$ point due to Van Hove singularities in the one-dimensional electronic density of states $D(E)$ of BN-SWNTs just at that point,

$$D(E) \propto \sum_{m=-(l-1)}^{l-1} G(E,\mathcal{E}_{m\pm}) \quad (38)$$

with

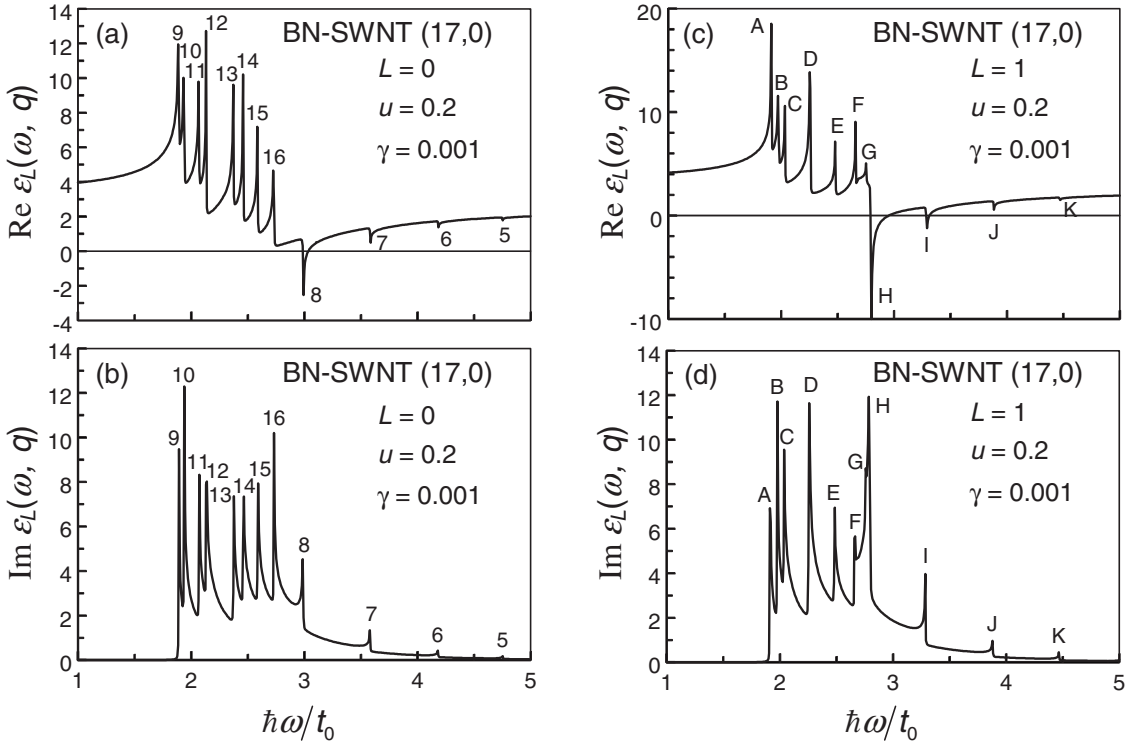

FIG. 3. The real and imaginary parts of the dielectric function $\varepsilon_L(\omega,q)$ are plotted versus $\hbar\omega/t_0$ for the BN-SWNT (17,0) at the value of the longitudinal momentum transfer q equal to $0.2k_{\mathrm{BZ}}$. The broadening parameter γ is chosen to be 0.001. The left (right) panels correspond to the angular momentum transfer $L=0(1)$. In panels (a) and (b), the numbers 5,6,…,16 on the top of the resonant and antiresonant peaks indicate the value of the azimuthal quantum number m corresponding to the single-particle interband excitation $v_m \rightarrow c_m$. In panels (c) and (d), the above-mentioned peaks are labeled by the capital alphabetic letters A,B,…,K. The correspondence between those letters and the interband transitions involved is as follows: A$-v_9\rightarrow c_{10}$, $v_{10}\rightarrow c_9$; B$-v_{10}\rightarrow c_{11}$, $v_{11}\rightarrow c_{10}$; C$-v_{11}\rightarrow c_{12}$, $v_{12}\rightarrow c_{11}$; D$-v_{12}\rightarrow c_{13}$, $v_{13}\rightarrow c_{12}$; E$-v_{13}\rightarrow c_{14}$, $v_{14}\rightarrow c_{13}$; F$-v_{14}\rightarrow c_{15}$, $v_{15}\rightarrow c_{14}$; G$-v_{15}\rightarrow c_{16}$, $v_{16}\rightarrow c_{15}$; H$-v_8\rightarrow c_9$, $v_9\rightarrow c_8$; I$-v_8\rightarrow c_7$, $v_7\rightarrow c_8$; J$-v_7\rightarrow c_6$, $v_6\rightarrow c_7$; K$-v_6\rightarrow c_5$, $v_5\rightarrow c_6$.

$$G(E,\mathcal{E}_{m\pm})=\begin{cases}\dfrac{|E|}{\sqrt{(E^2-\mathcal{E}_{m-}^2)(\mathcal{E}_{m+}^2-E^2)}} & \text{for } |\mathcal{E}_{m-}|<|E|<|\mathcal{E}_{m+}| \\ 0 & \text{for } |E|<|\mathcal{E}_{m-}|,|E|>|\mathcal{E}_{m+}|,\end{cases} \tag{39}$$

where

$$\mathcal{E}_{m\pm}^2=\Delta^2+t_0^2(1\pm 2|\nu_m|)^2. \tag{40}$$

The above-mentioned interband excitations induce rich resonant structures in the spectra of the imaginary part of $\varepsilon_L(\omega,q)$, as is seen from Figs. 3(b) and 3(d). In Fig. 3(b), where the spectrum of Im $\varepsilon_L(\omega,q)$ with $L=0$ is plotted, the peaks corresponding to the excitations $v_m\rightarrow c_m$ are marked with the number $m=5,6,\ldots,16$ on the top of the peaks. The labeling of the individual peaks in that spectrum is based on the systematics of the energy subbands summarized in Sec. II A. With this systematics, the index $|m|=m_g$ [equal to 9 for the BN-SWNT (17,0)] is attributed to the innermost symmetric pair of normally dispersed (i.e., dispersed upward) subbands followed by (in sequential order) the other pairs of normally dispersed subbands with $|m|>m_g$ up to $|m|=l-1$ (equal to 16 in the case under discussion). The next pair of the subbands, which are already dispersed anomalously (i.e., downward), corresponds to $|m|=m_p<l-1$ with m_p defined as

$$m_p=m_g-1=[l/2], \tag{41}$$

where the square brackets denote, as in Eq. (20), the integral part of the number they contain in. So far as the BN-SWNT (17,0) is concerned, $m_p=8$. It follows from Eqs. (38)–(40) that the density of states $D(E)$ is divergent in $1/\sqrt{E-\mathcal{E}_{m-}}$ form for $|m|>m_p$, i.e., for the subbands dispersed normally, whereas it diverges in reverse $1/\sqrt{\mathcal{E}_{m+}-E}$ form for $|m|\leqslant m_p$, i.e., for the subbands dispersed anomalously. Since the imaginary part of the dielectric function in the limit $\Gamma\rightarrow 0$ is proportional to the density of states, the above considerations account for the difference in the profile of the peaks with $|m|>m_p$ and $|m|\leqslant m_p$, which can be seen in Figs. 3(b) and

3(d). Indeed, the left-hand side of the peaks with $|m|>m_p$ is almost vertical, whereas their right-hand side is somewhat more slanting, and vice versa for the peaks with $|m|\leqslant m_p$. There is one more point to note regarding the peaks with $|m|>m_p$ and $|m|\leqslant m_p$ in the spectra of $\mathrm{Im}\,\varepsilon_L(\omega,q)$. Namely, some of the former peaks are very closely spaced, so that, if the width of the peaks, Γ, is larger, they will begin to merge. As a result, the number of the resolved peaks with $|m|>m_p$ can be smaller than that revealed in the spectra of $\mathrm{Im}\,\varepsilon_L(\omega,q)$ in Figs. 3(b) and 3(d). In this connection it is worthwhile to remind the reader that Γ is treated as a free parameter here and its value $\hbar\Gamma=2.4$ meV, used in the above calculations, is chosen only in order to clarify the basic features of the dielectric function before a more realistic choice of the Γ value will be made (see further below). As to the peaks with $|m|\leqslant m_p$, they are much more rarefied than those with $|m|>m_p$, which directly reflects the larger energy spacing between the corresponding nearest-neighbor subbands in this case (see Fig. 2). Besides, the amplitudes of the peaks with $|m|\leqslant m_p$, being considerably smaller than those of the peaks with $|m|>m_p$, fall off rapidly as $\hbar\omega/t_0$ increases, so that the spectra of $\mathrm{Im}\,\varepsilon_L(\omega,q)$ become essentially featureless above $\hbar\Gamma/t_0\simeq 5$. This implies that the excitations associated with the π-band electrons almost disappear there.

Turning now to the spectra $\mathrm{Re}\,\varepsilon_L(\omega,q)$ shown in Figs. 3(a) and 3(c), it should be noted that their basic features can easily be understood if one takes into account that the real and the imaginary parts of $\varepsilon_L(\omega,q)$ are connected with each other by the Kramers-Kronig relation at every fixed value of q.[42] In consequence, the "resonant" and "antiresonant" (dip) structures, observed in those figures, appear just in the neighborhood of the resonances in the imaginary part of $\varepsilon_L(\omega,q)$. Therefore, in Fig. 3(a) these structures are labeled by the same index m as the resonant peaks in Fig. 3(b). It is also evident that in the near vicinity of the frequencies where $\mathrm{Im}\,\varepsilon_L(\omega,q)$ is picked, the real part of $\varepsilon_L(\omega,q)$ can change its sign (from positive to negative and vice versa), passing through zero. As is well known, the roots of the equation

$$\mathrm{Re}\,\varepsilon_L(\omega,q)=0 \tag{42}$$

determine the frequencies $\omega_L^{(i)}(q)$ of the plasmon modes of the system, the superscript $i=1,2,3,\ldots$ indexing the branches of the plasmon spectrum. In the case under consideration, these modes represent the self-sustaining coherent oscillations of the electron charge density associated with interband π-electronic excitations. The condition for such oscillations to be long-lived and hence well-defined collective excitations of the system requires the following inequality to be satisfied:

$$\omega_L^{(i)}(q)\gg\Gamma_L^{(i)}(q), \tag{43}$$

where $\Gamma_L^{(i)}(q)>0$ is the lifetime of the excitations due to the so-called dephasing processes that affect only the relative phases of the many-particle eigenstates of the system without resulting in energy relaxation. In a weak-damping case, $\Gamma_L^{(i)}\times(q)$ is approximated by

$$\Gamma_L^{(i)}(q)=\mathrm{Im}\,\varepsilon_L(\omega,q)/\partial[\mathrm{Re}\,\varepsilon_L(\omega,q)]/\partial\omega|_{\omega=\omega_L^{(i)}(q)}. \tag{44}$$

This equation can scarcely be used directly to check the validity of the initial assumption, given by Eq. (43), that the damping is do small. The point is that one cannot derive the plasmon dispersion $\omega_L^{(i)}(q)$ in an explicit analytic form by solving Eq. (42), mainly because the integral in Eq. (29) for $\mathrm{Re}\,\varepsilon_L(\omega,q)$ cannot be evaluated analytically. Therefore, Eq. (42) should be solved either numerically or graphically. It is the last means that we will further resort to in order to obtain the plasmon dispersion relation $\omega_L(q)$. In this context, Eq. (44) turns out to be very useful because, along with Eq. (43), it indicates that the solutions of Eq. (42) corresponding to plasmons should be looked for in the frequency region where the imaginary part of $\varepsilon_L(\omega,q)$ is not large and, simultaneously, the derivative entering Eq. (44) is positive.

It is worthwhile to note that, in principle, there is one more means that could be applied in order to determine the dispersion $\omega_L^{(i)}(q)$ and the lifetime $\Gamma_L^{(i)}(q)$ of different plasmon modes. As is known, well-defined plasmon modes are associated with resonances in the so-called electron-energy-loss function

$$S_L(\omega,q)=\mathrm{Im}\left[-\frac{1}{\varepsilon_L(\omega,q)}\right]=\frac{\mathrm{Im}\,\varepsilon_L(\omega,q)}{[\mathrm{Re}\,\varepsilon_L(\omega,q)]^2+[\mathrm{Im}\,\varepsilon_L(\omega,q)]^2}, \tag{45}$$

which is of primary interest for us here, since it is just this function that is measured in EELS experiments. Both the above-mentioned quantities, $\omega_L^{(i)}(q)$ and $\Gamma_L^{(i)}(q)$, can then be directly determined from the plot of S_L as a function of ω at a given value of q by finding the positions of the peaks and the half-width of the peaks at half maximum, which yields $\omega_L^{(i)}(q)$ and $\Gamma_L^{(i)}(q)$, respectively. Such an approach generally assumes that all the peaks in the loss-function spectrum can be attributed to plasmons. This is, however, not the case, and the above spectrum can exhibit the resonant structures, which have a different origin, not associated with the zeros of $\mathrm{Re}\,\varepsilon_L(\omega,q)$, i.e., with the plasmons. In order to understand the origin of such structures, which can appear in the low-energy region of the $S_L(\omega,q)$ spectra at fairly small γ values (see Fig. 5 further below), we have to address ourselves to Fig. 3(a) that demonstrates the distinctive resonant structures with $m=9-16$ at low energies ($\hbar\omega/t_0<2.7$). In this region, it can also be seen local minima situated between neighboring sharp peaks, neither of the minima reaching zero. We would like to emphasize that such behavior of $\mathrm{Re}\,\varepsilon_L(\omega,q)$ is quite insensitive to the value of γ used in the calculation and should be expected no matter how small (but finite) the value of γ is. The reason for this is easy to perceive if one notices that in the limit $\gamma\to 0$ the real part of $\varepsilon_L(\omega,q)$ is divergent at resonant frequencies where $\mathrm{Im}\,\varepsilon_L(\omega,q)$ has δ-like peaks. In the near vicinity of those frequencies, the $\mathrm{Re}\,\varepsilon_L(\omega,q)$ goes to $+\infty(-\infty)$ as the frequency approaches the resonant value from the left (right). In the case of a nonzero, but weak broadening ($0<\gamma\ll 1$), the real part of $\varepsilon_L(\omega,q)$, instead of having discontinuity at the resonant frequencies, passes through zero there, drastically changing from large positive values to large

negative ones in the vicinity of those frequencies. Therefore, if these resonant frequencies were wide spaced, there might be a number of low-energy plasmon modes associated with the zeros of the Re $\varepsilon_L(\omega,q)$ in this region. This is, however, not the case, and the nearest-neighboring resonant frequencies are sufficiently close to one another because of very small energy spacing (around $k=0$) between the nearest-neighboring subbands dispersed normally (see Fig. 2). The individual frequency-dispersion curves of the Re $\varepsilon_L(\omega,q)$, corresponding to each of the broadened resonances in the Im $\varepsilon_L(\omega,q)$, essentially overlap and, as a result, the real part of $\varepsilon_L(\omega,q)$ becomes positive throughout the whole low-energy region, where m varies from 9 to 16, no longer vanishing in this region and exhibiting local minima instead of the zeros. It is quite clear, therefore, that the resonant structures, appearing in the low-energy region of the $S_L(\omega,q)$ spectra, may not at all be associated with plasmons, corresponding to the zeros of the Re $\varepsilon_L(\omega,q)$, but can simply reflect the presence of different real roots of the equation

$$\{[\mathrm{Re}\ \varepsilon_L(\omega,q)]^2 - [\mathrm{Im}\ \varepsilon_L(\omega,q)]^2\}\partial\ \mathrm{Im}\ \varepsilon_L(\omega,q)/\partial\omega - 2\ \mathrm{Re}\ \varepsilon_L(\omega,q)\mathrm{Im}\ \varepsilon_L(\omega,q)\partial\ \mathrm{Re}\ \varepsilon_L(\omega,q)/\partial\omega = 0, \tag{46}$$

which represents the necessary condition for $S_L(\omega,q)$ of Eq. (45) to have extremum points. This implies that considerable care has to be taken in the interpretation of the low-energy resonant structures in the $S_L(\omega,q)$ spectra.[43] In order to avoid misinterpretation, it is preferable, at least from the theoretical standpoint, to determine the frequencies of plasmon modes directly from Eq. (42).

From the graph of Re $\varepsilon_L(\omega,q)$ in Fig. 3(a), it is seen that the Re $\varepsilon_L(\omega,q)$ vanishes only if m is equal to m_p defined by Eq. (41). Physically, this may be thought of as resulting from the excitation of the collective electronic mode associated with interband electron transitions between energy subbands dispersed downward (see Fig. 2). There are two main reasons for Re $\varepsilon_L(\omega,q)$ to exhibit an antiresonant (dip) structure [with vanishing Re $\varepsilon_L(\omega,q)$] when the above-mentioned transitions are involved. The first of them is easy to understand if we turn again to the limit of zero-broadening ($\gamma \to 0$). In the near vicinity of the resonant frequency, the Re $\varepsilon_L(\omega,q)$ is then divergent in reverse form as compared to that we pointed out above in discussing the behavior of Re $\varepsilon_L(\omega,q)$ in the low-energy region. Namely, since the subbands under consideration are dispersed anomalously, the Re $\varepsilon_L(\omega,q)$ goes to $-\infty(+\infty)$ as the frequency approaches the resonant value from the left (right). When the broadening effect is finite but weak ($0<\gamma\ll 1$), this divergent structure is somewhat smeared out, yet its basic feature remains unchanged, namely, the Re $\varepsilon_L(\omega,q)$ varies drastically from a large negative value to a large positive one, passing through zero at the resonant frequency. The second of the above-mentioned reasons is that the energy spacing (around $k=0$) between the last subband dispersed upward ($m=l-1$) and the subsequent subband dispersed downward ($m=m_p$) is large enough so as the first dip structure in the Re $\varepsilon_L(\omega,q)$ spectrum should not be suppressed by the last peak structure in the same spectrum. The left wing of the dip structure superimposed on the right wing of the peak structure produces a distinctive shoulder at $\hbar\omega/t_0=2.6-2.7$ in the Re $\varepsilon_L(\omega,q)$ spectrum in Fig. 3(a). Such a shoulder is a precursor for Re $\varepsilon_L(\omega,q)$ to become zero for the first time. Note that the other dip structures (with $m=7$, 6, and 5) in Fig. 3(a) are less pronounced and none of them leads to the vanishing Re $\varepsilon_L(\omega,q)$. This implies that only one $L=0$ plasmon mode can exist at the values of q and γ given in Fig. 3(a). If they are different from those indicated in Fig. 3(a), then the situation could, in principle, change drastically, and there could be a number of plasmon modes associated with the zeros of Re $\varepsilon_L(\omega,q)$, originating from the dip structures with $m=7,6,5$, etc.

Our calculations show that even at the same values of q and γ as in Fig. 3(a), the number of the plasmon modes can be more than one if $L\neq 0$. The spectra of the real and the imaginary parts of $\varepsilon_L(\omega,q)$ for $L=1$ are shown in Figs. 3(c) and 3(d), respectively. The resonant and antiresonant structures in those figures, corresponding to the interband excitations $v_m \to c_{m+1}$, are marked with capital letters of the Latin alphabet (for details, see the caption in Fig. 3). Comparing the graphs in Figs. 3(a) and 3(c), we can conclude that the spectra of Re $\varepsilon_L(\omega,q)$ for the cases $L=0$ and $L=1$, being overall similar in structure, differ from each other in one important point, namely, there are two dip structures with the vanishing Re $\varepsilon_L(\omega,q)$ for $L=1$ in contrast to the one such structure in the $L=0$ case, and hence, in general, two $L=1$ plasmon modes can exist at the given values of q and γ.

As remarked earlier, the existence of long-lived plasmon modes requires that their frequencies must be out of the region where Im $\varepsilon_L(\omega,q)$ is large. It is also necessary that $\Gamma_L^{(i)}(q)$ of Eq. (44) should be positive. In Fig. 4, which is the complement of Figs. 3(a) and 3(b), we show the details of the behavior of Re $\varepsilon_L(\omega,q)$ and Im $\varepsilon_L(\omega,q)$ for $L=0$ in the region where the graph of Re $\varepsilon_L(\omega,q)$ passes through zero. Note that Re $\varepsilon_L(\omega,q)$ vanishes two times in this region, and such behavior is a typical one for other dip structures with the vanishing Re $\varepsilon_L(\omega,q)$. However, the zero on the left-hand side (lower energy) of the dip structure, marked with an open circle in Fig. 4, does not correspond to a collective mode in any sense because both of the aforesaid requirements are not satisfied at that point. On the contrary, these requirements are apparently fulfilled for the zero situated on the right-hand side of the dip structure and marked with a solid circle in Fig. 4. Therefore, it is this second zero that may be recognized as corresponding to a well-defined collective electronic mode of the system. The energy of this only possible $L=0$ plasmon mode at $q=0$ is close to the energy separation (at $k=0$) between the two subbands with $m=m_p$—one in the v band and the other in the c band—and, hence, can be approximated as

$$\hbar\omega_{L=0}^{(i=1)}(q=0) \approx 2\sqrt{\Delta^2 + t_0^2(1+2\nu_{m_p})^2}, \tag{47}$$

where

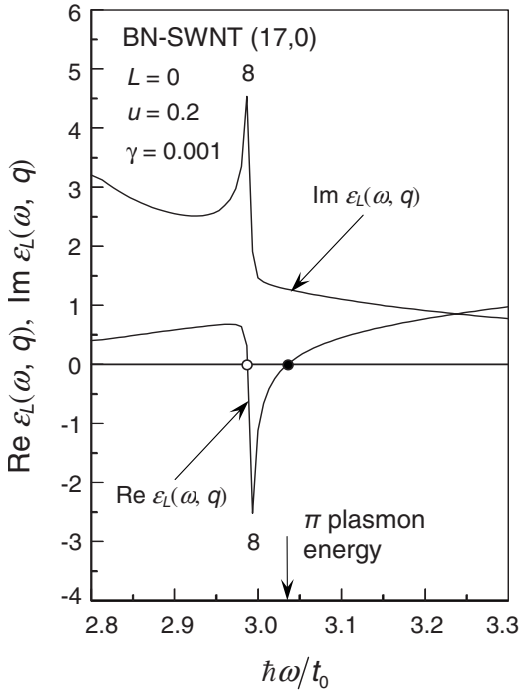

FIG. 4. Plot of the real and the imaginary parts of the dielectric function $\varepsilon_L(\omega,q)$ versus $\hbar\omega/t_0$ for the BN-SWNT (17,0) in the region where the Re $\varepsilon_L(\omega,q)$ vanishes. The momentum transfer q and the parameter γ are the same as in Fig. 3. The angular momentum transfer $L=0$. The open and solid circles mark the zeros of Re $\varepsilon_L(\omega,q)$. The arrow on the horizontal axis indicates the location of the π plasmon energy. Number 8 on the top of the resonant and antiresonant peaks indicates the value of the azimuthal quantum number m_p (see the captions in Figs. 2 and 3).

$$\nu_{m_p} = \cos(\pi m_p/l) \tag{48}$$

with m_p defined by Eq. (41). We would like to emphasize that the collective nature of the interband plasmon mode we consider implies that its energy is, in fact, slightly shifted from the single-particle interband transition energy determined by Eq. (47). Yet the magnitude of the shift cannot be derived analytically even in the long-wavelength limit ($q \to 0$), to say nothing of the plasmon frequency away from this limit, where only numerical results can be obtained.

We now turn to a series of specific examples that illustrate the behavior of the electron-energy-loss function $S_L(\omega,q)$ defined by Eq. (45). All these are relevant to the three individual BN-SWNTs with indices (17,0), (21,0), and (25,0).

Our first example, presented in Fig. 5, shows the frequency variation of the loss-function $S_L(\omega,q)$ for three values of the broadening parameter γ and fixed L and q ($L=0$, $q=0.3k_{\mathrm{BZ}}$). For the smallest values of γ displayed in that figure, each of the calculated spectra is seen to be dominated by the pronounced and rather broad resonant peak marked with the capital letter P. The position of the peak, as given by the root of Eq. (42) at $L=0$, allows one to attribute it to the $L=0$ plasmon mode. As can be seen from Fig. 5, there is a number of very sharp and well-separated peaks situated on the right of the dominant plasmon peak, their intensity falling off rapidly on going to the high energies. These peaks, as

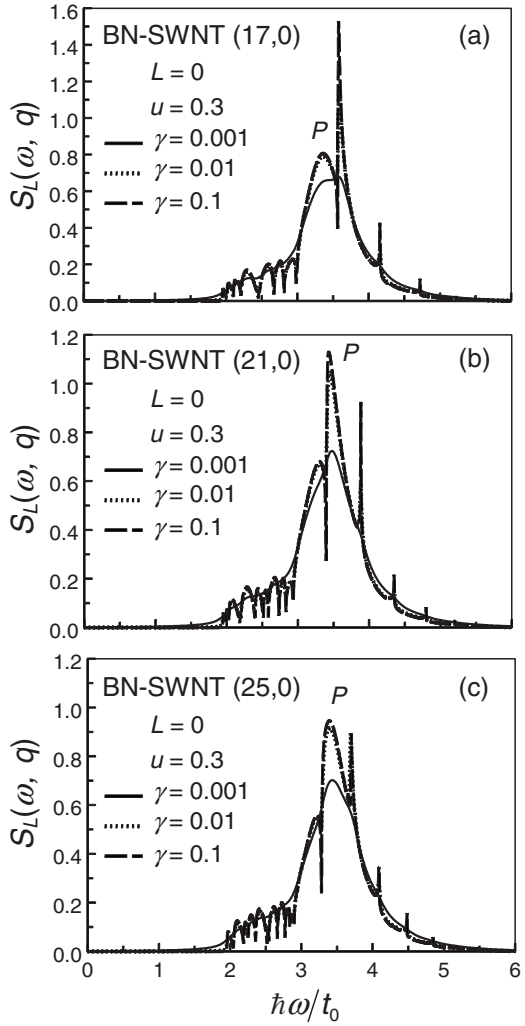

FIG. 5. The calculated electron-energy-loss function $S_L(\omega,q)$ is plotted versus $\hbar\omega/t_0$ at zero angular momentum transfer ($L=0$) for the BN-SWNTs (17,0) (a), (21,0) (b), and (25,0) (c) at the three different values of the broadening parameter γ given in the figure.

well as numerous very closely spaced characteristic features on the left of the main plasmon peak, are associated with the roots of Eq. (46) different from those of Eq. (42) and, hence, do not originate from plasmons. As γ increases, all these nonplasmonic resonant structures are smeared out because of the broadening, so that at $\gamma=0.1$ they completely disappear and the broadened plasmon peak remains the only dominating resonant structure in the spectra. In this connection, it is worthwhile to note that in calculating the spectra of Re $\varepsilon_L(\omega,q)$ and Im $\varepsilon_L(\omega,q)$ in Fig. 3 we have chosen $\gamma=0.001$ because we aimed to demonstrate all the basic features of the spectra as clear as possible. That values of γ, however, appear to be too small considering how broad the plasmon structure in the experimentally observed electron-energy-loss spectra[19] is. In order to make a comparison with experiment more meaningful, it seems to be reasonable to pick up more strong broadening. It is for this reason that we take the value of γ at 0.08 as input of our numerical calculations of the $S_L(\omega,q)$ spectra shown in Figs. 6 and 7.

In Fig. 6, we plot the frequency variation of $S_L(\omega,q)$ for four different values of the angular momentum transfer L at

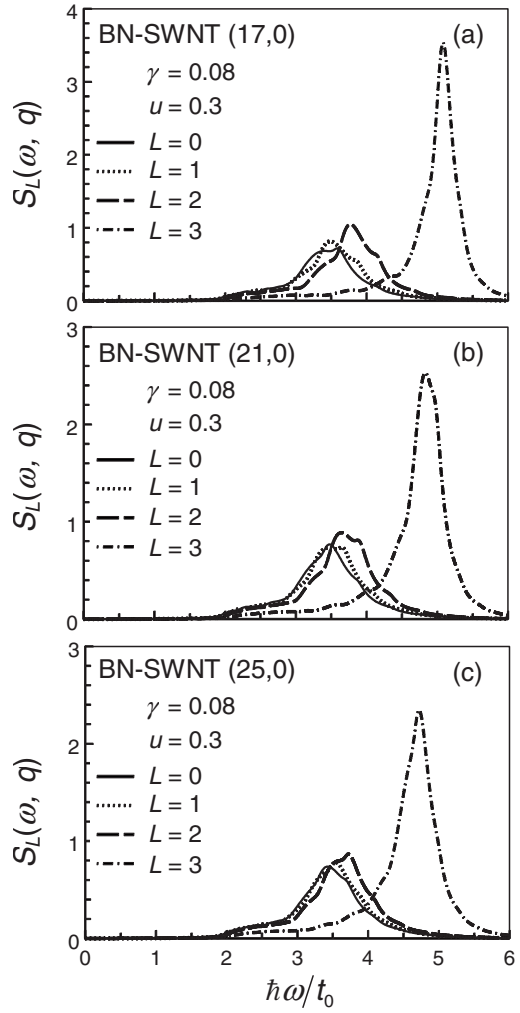

FIG. 6. The calculated electron-energy-loss spectra $S_L(\omega,q)$ for the BN-SWNTs (17,0) (a), (21,0) (b), and (25,0) (c) at the transferred momentum $q=0.3k_{BZ}$ and the four different values of the angular transferred momentum $L(=0,1,2,3)$. The broadening parameter γ is equal to 0.08.

fixed $q=0.3k_{BZ}$. We find that each of the spectra is dominated by only a single, prominent resonant peak structure, produced by the corresponding $L(=0,1,2,3)$ plasmon mode. The peaks of the function $S_L(\omega,q)$ are clearly shifted to higher energies with increasing L and, hence, so do the π-plasmon frequencies, the plasmon with a higher frequency producing a higher peak in the spectra. There is also an appreciable shift of the $L=3$ π-plasmon peak to lower energies on going over to larger nanotubes, whereas the positions of the peaks corresponding to the $L=0,1,2$ plasmons are practically independent of the nanotube radius. In addition, the larger is the nanotube radius, the lower is the height of the peak originated from the $L=3$ plasmon, while the effect of the nanotube radius on the height of the peaks corresponding to the $L=0,1,2$ plasmons is again very weak.

The fact that the peaks with larger L are located at higher energies and have larger height is quite clear physically. The blueshift of the peaks with increasing L directly reflects the growth of the minimal energy required for the π electrons to be excited from the subbands dispersed upward in the v band to those dispersed downward in the c band. As remarked earlier, only if such single-particle excitations are involved, the real part of $\varepsilon_L(\omega,q)$ may be expected to become zero in the region where its imaginary part is small enough.

As to the enhancement of the height of the plasmon peaks with increasing L, the main reason for this is that the probability of the interband excitations induced by the self-consistent potential, inherent in the system under consideration, decreases with an increase in L. This behavior correlates with expectation, based on physical grounds, that the oscillator strength of multipole modes $(L\neq 0)$ will be smaller than that of the principle mode with $L=0$. Remembering that at the plasmon frequency the loss-function $S_L(\omega,q)$ of Eq. (45) is inversely proportional to the $\mathrm{Im}\,\varepsilon_L(\omega,q)$, which in turn is proportional to the above-mentioned probability, it becomes clear that at larger L the peaks in the $S_L(\omega,q)$ spectra will have the larger height.

The aforementioned nonsensitivity of the spectra $S_L(\omega,q)$ at small L to the size of the nanotubes also allows a simple qualitative explanation. Plasmons are quanta of the collective excitations of the electron density of the nanotubes. The $L=0$ plasmons correspond to density oscillations along the nanotube axis, and therefore it is not surprising that, as such, they are unaffected by the nanotube radius at all. On the contrary, the $L\neq 0$ plasmons correspond to mixed density oscillations, which include rotational charge density oscillations around the nanotube. The effect of this extra transverse component of the oscillations is weak at small L, but it evidently increases with increasing L and at $L\geqslant 3$ it becomes appreciable, as we can see from Fig. 6.

Figure 7 displays the frequency variation of the loss-function $S_L(\omega,q)$ with $L=0$ (left panels) and $L=1$ (right panels) for four different q's. For all the spectra shown in that figure, we again find only a single prominent loss peak, corresponding to the π plasmon at the given L, with no evidence of contributions from extra plasmon modes with lower energies, a result we have commented on earlier in this paper. We also see that the position of the loss peak in the spectra depends on the transferred momentum q, suffering a blueshift with increasing q. However, the magnitude of the shift is not too large, which implies that the momentum dependence of the $L=0,1$ π-plasmon frequencies is rather weak. Besides, as has already been previously explained, a similar weak dispersion should be expected for the frequency of the $L=2$ plasmon. Indeed, this physical picture is well supported by the numerical results shown in Fig. 8, where the dispersion curves for the $L=0,1,2,3$ plasmons in the three individual BN-SWNTs under consideration are presented. The curves have been obtained by scanning both the real and the imaginary parts of $\varepsilon_L(\omega,q)$ as a function of frequency in order to find where the zeros of the $\mathrm{Re}\,\varepsilon_L(\omega,q)$ for different q's are located provided that the $\mathrm{Im}\,\varepsilon_L(\omega,q)$ is simultaneously small.

The most important message of Fig. 8 is that the π-plasmon spectrum of the BN-SWNTs consists of the several branches none of which start from $q=0$ but apparently approaches this point with increasing L. This result is nontrivial and, as far as we know, has never been previously reported for other nanometer-sized tubular systems, such as,

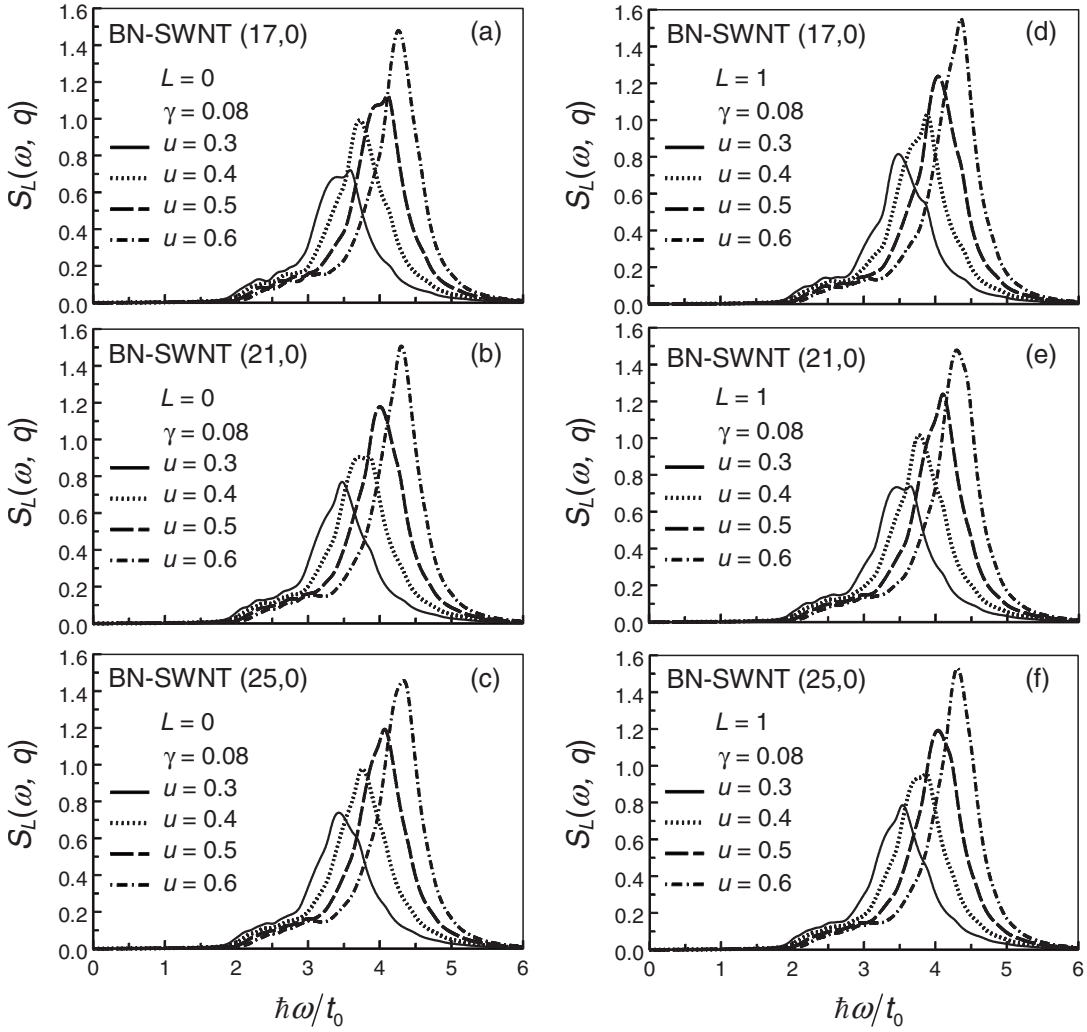

FIG. 7. The calculated electron-energy-loss spectra $S_L(\omega,q)$ for the BN-SWNTs (17,0) [(a) and (d)], (21,0) [(b) and (e)], and (25,0) [(c) and (f)] at $L=0$ (left panels) and $L=1$ (right panels). The solid, dotted, dashed, and dot-dashed curves on each panel correspond to the four values of the transferred momentum $q=0.3k_{BZ}$, $0.4k_{BZ}$, $0.5k_{BZ}$, and $0.6k_{BZ}$, respectively. The broadening parameter γ is equal to 0.08.

e.g., CNTs (see Ref. 24). Certainly, one cannot rule out the existence of other plasmons with $L>3$ in the limit $q\rightarrow 0$, but, as remarked earlier, their oscillator strength will inevitably be smaller than that of the plasmon modes with $L=0,1,2,3$.

It is worthwhile to note another result that follows from the graphs in Fig. 8, namely, the q dependence of the plasmon frequencies is virtually linear at large q for all the branches plotted in that figure. One more important trend, which is evident from Fig. 8, is that the $L=0,1,2$ plasmon dispersion curves converge to the same value with increasing q, the branches with $L=0$ and $L=1$ practically merging already starting from $q=0.3k_{BZ}$. The last feature implies that it may at least be extremely hard, if not impossible to distinguish those plasmon modes in experiment, even if one uses the momentum-resolved EELS method.

The above discussion also indicates that considerable care has to be taken in the interpretation of the EELS experiment by Arenal *et al.*,[19] as however, mentioned by themselves. From Fig. 8 we find that the π-plasmon frequency should be approximately 6–7 eV at small q's and L's, if we take $t_0=2.4$ eV, as has been adopted above. This could explain the measured plasmon frequency of about 6.6–6.9 eV in the experiment of Arenal *et al.*[19] However, in view of the specific structure of the π-plasmon spectrum mentioned above, it is necessary to have full momentum-resolved capability to obtain information on transfer-momentum-dependent features in electron-energy-loss spectra such as studied in the present paper. This would provide direct experimental access to the dispersion of the π plasmons in BN-SWNTs obtained in our calculations. There are a number of predictions in this paper, with regard to the plasmon dispersion, which are, in principle, experimentally testable, if the above-mentioned spectroscopy studies were carried out. One of the most interesting among them is that only the $L=3$ branch of the plasmon spectrum experiences an appreciable redshift with increasing the nanotube radius, whereas the energies of the three lowest plasmon modes, including the principle mode with $L=0$, are insensitive to the size of the nanotubes. One more significant conclusion which can be drawn from Fig. 8 is that all the plasmon mode branches in that figure display a weak positive dispersion, i.e., they disperse upward as q increases.

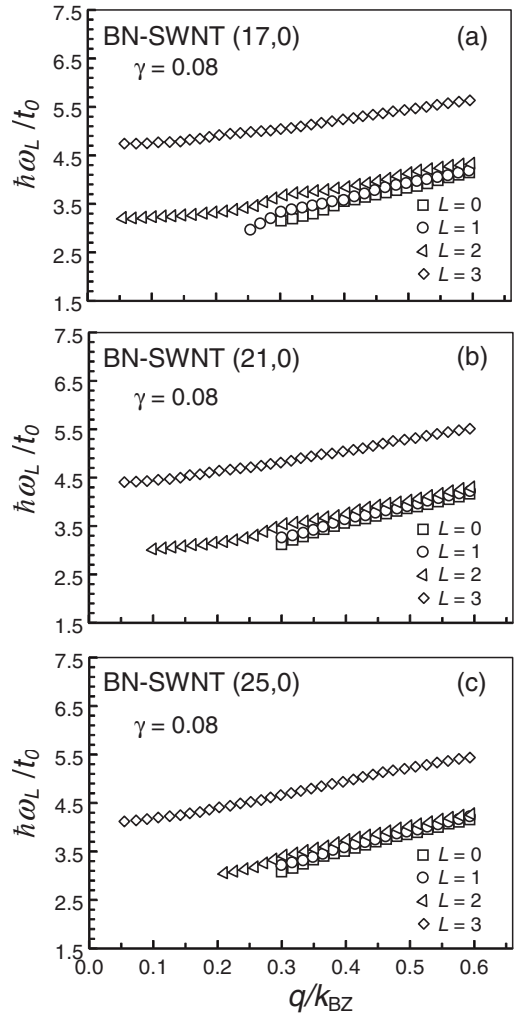

FIG. 8. The calculated dispersion curves for the $L=0,1,2,3$ π-plasmon modes in the BN-SWNTs (17,0) (a), (21,0) (b), and (25,0) (c) are shown by open squares, circles, triangles, and diamonds, respectively.

This result is in good qualitative agreement with the experiment of Fuentes *et al.*,[18] although a fully quantitative comparison between our calculated results and that experiment seems to be impossible because the measurements in Ref. 18 were carried out on BN-MWNTs and the direct applicability of our theory to such nanotubes is questionable. An extension of the theory to study BN-MWNTs would therefore be of very great interest. Such an extension will be presented in a separate paper.

IV. CONCLUSIONS

In this paper, we have presented a comprehensive theory of the dynamic dielectric response of individual zigzag BN-SWNTs, developed on the basis of the self-consistent-field approximation of Ehrenreich and Cohen.[22] The electronic structure of the nanotubes has been calculated using a simple two-band π-orbital TB Hamiltonian that describes the energy bands of such tubes via two model parameters. Within this approach, we have derived an analytical expression for the longitudinal dielectric function of the BN-SWNTs, which could be useful in calculating different characteristics relevant to the dielectric properties of these tubes.

The application of the dielectric function in the present paper has been directed to the study of the electron-energy-loss spectra and the collective electronic excitations (plasmons) in the BN-SWNTs. Our calculations have shown that each of the tubes supports only one branch of the wave-number-dispersed collective π-plasmon mode for each transferred quantum angular momentum L. The branches corresponding to different L's are shown to display unusual dispersion characteristics due to the unique features of the considered class of nanotubes. In particular, we have found that none of the branches start from the zero value of the transferred momentum q, at least at the value of the broadening parameter, which is chosen as being realistic enough for the nanotubes under consideration. This means that one should be cautioned in interpreting the non-momentum-resolved EELS experiments of the type carried out by Arenal *et al.*[19] It is evidently difficult to extract reliable information on the plasmon frequencies from such experiments. On the other hand, to the best of our knowledge, no momentum-resolved EELS measurements on individual BN-SWNTs have been made so far. We hope that the results of the present paper will stimulate experimental interest in this topic.

ACKNOWLEDGMENTS

This work has been supported by a grant from the Russian Foundation for Basic Research. We would like to thank M. F. Lin for having sent us the reprints of his papers on plasmons in CNTs. We are also indebted to R. Perez for supplying us with an electronic copy of his paper (Ref. 24).

*Author to whom correspondence should be addressed. Mailing address: Sovetskaya 31, kv. 32, Saransk 430000, Russia. 612033@inbox.ru

[1] A. Rubio, J. L. Corkill, and M. L. Cohen, Phys. Rev. B **49**, 5081 (1994).

[2] R. Saito, G. Dresselhaus, and M. S. Dresselhaus, *Physical Properties of Carbon Nanotubes* (Imperial College Press, London, 1998).

[3] M. Terrones, J. M. Romo-Herrera, E. Cruz-Silva, F. López-Urias, E. Muñoz-Sandoval, J. J. Velázquez-Salazar, H. Terrones, Y. Bando, and D. Golberg, Mater. Today **10**, 30 (2007).

[4] X. Blase, A. Rubio, S. G. Louie, and M. L. Cohen, Europhys. Lett. **5**, 335 (1994).

[5] E. Hernández, C. Goze, P. Bernier, and A. Rubio, Phys. Rev. Lett. **80**, 4502 (1998).

[6] N. G. Chopra and A. Zettl, Solid State Commun. **105**, 297

(1998).
[7] P. Zhang and V. H. Crespi, Phys. Rev. B **62**, 11050 (2000).
[8] K. N. Kudin, G. E. Scuseria, and B. I. Yakobson, Phys. Rev. B **64**, 235406 (2001).
[9] H. F. Bettinger, T. Dumitrică, G. E. Scuseria, and B. I. Yakobson, Phys. Rev. B **65**, 041406(R) (2002).
[10] A. B. Suryavanshi, M.-F. Yu, J. Wen, C. Tang, and Y. Bando, Appl. Phys. Lett. **84**, 2527 (2004).
[11] E. J. Mele and P. Král, Phys. Rev. Lett. **88**, 056803 (2002).
[12] S. M. Nakhmanson, A. Calzolari, V. Meunier, J. Bernholc, and M. B. Nardelli, Phys. Rev. B **67**, 235406 (2003).
[13] Y. Chen, J. Zou, S. J. Campbel, and G. L. Caer, Appl. Phys. Lett. **84**, 2430 (2004).
[14] W. Q. Han, W. Michalson, J. Cumings, and A. Zettl, Appl. Phys. Lett. **81**, 1110 (2002).
[15] A. Loiseau, F. Willaime, N. Demoncy, G. Hug, and H. Pascard, Phys. Rev. Lett. **76**, 4737 (1996).
[16] M. Terauchi, M. Tanaka, T. Matsumoto, and Y. Saito, J. Electron Microsc. **47**, 319 (1998).
[17] M. Kociak, L. Henrard, O. Stéphan, K. Suenaga, and C. Colliex, Phys. Rev. B **61**, 13936 (2000).
[18] G. G. Fuentes, E. Borowiak-Palen, T. Pichler, X. Liu, A. Graff, G. Behr, R. J. Kalenczuk, M. Knupfer, and J. Fink, Phys. Rev. B **67**, 035429 (2003).
[19] R. Arenal, O. Stéphan, M. Kociak, D. Taverna, A. Loiseau, and C. Colliex, Phys. Rev. Lett. **95**, 127601 (2005).
[20] A. G. Marinopoulos, L. Wirtz, A. Marini, V. Olevano, A. Rubio, and L. Reining, Appl. Phys. A: Mater. Sci. Process. **78**, 1157 (2004).
[21] G. Y. Guo and J. C. Lin, Phys. Rev. B **71**, 165402 (2005).
[22] H. Ehrenreich and M. H. Cohen, Phys. Rev. **115**, 786 (1959).
[23] M. F. Lin, D. S. Chuu, C. S. Huang, Y. K. Lin, and K. W.-K. Shung, Phys. Rev. B **53**, 15493 (1996).
[24] R. Perez and W. Que, J. Phys.: Condens. Matter **18**, 3197 (2006).
[25] Vl. A. Margulis, E. A. Gaiduk, E. E. Muryumin, O. V. Boyarkina, and L. V. Fomina, Phys. Rev. B **74**, 245419 (2006).
[26] M. Therauchi, M. Tanaka, K. Suzuki, A. Ogino, and K. Kimura, Chem. Phys. Lett. **324**, 359 (2000).
[27] R. S. Lee, J. Gavillet, M. Lamy de la Chapelle, A. Loiseau, J.-L. Cochon, D. Pigache, J. Thibault, and F. Willaime, Phys. Rev. B **64**, 121405(R) (2001).
[28] A simple model of the electronic structure of BN-SWNTs has recently been proposed by P. Král, E. J. Mele, and D. Tomanek, Phys. Rev. Lett. **85**, 1512 (2000). Their rather elegant analytical approach is based on an effective-mass approximation and, as such, is valid only in the vicinity of the extrema of the energy bands. This approach can provide a reasonably good description of a number of phenomena in BN-SWNTs, such as, for example, spontaneous polarization (Ref. 11) or optical absorption (Ref. 25), which are dominated by the electronic states near those extrema. However, for the reasons indicated in Sec. II B of the main text, a more general study of the electronic structure of BN-SWNTs has to be used in the description of the collective electronic exitations in these nanotubes. The presence of the energy subbands, dispersed upward and downward in both the v and c bands, plays the key role here, whereas this basic feature is missing in a simple $\mathbf{k}\cdot\mathbf{p}$ band structure model used by Král *et al.* in their perspective paper cited above.
[29] E. M. Lifshitz and L. P. Pitaevskii, *Statistical Physics* (Pergamon, New York, 1980), Pt. 2, Sec. 55.
[30] J. S. Lauret, R. Arenal, F. Ducastelle, A. Loiseau, M. Cau, B. Attal-Tretout, and E. Rosencher, Phys. Rev. Lett. **94**, 037405 (2005).
[31] J. Wang, V. K. Kayastha, Y. K. Yap, Z. Fan, J. G. Lu, Z. Pan, I. N. Ivanov, A. A. Puretzky, and D. B. Geohegan, Nano Lett. **5**, 2528 (2005).
[32] S. Okada, S. Saito, and A. Oshiyama, Phys. Rev. B **65**, 165410 (2002).
[33] T. M. Schmidt, R. J. Baierle, P. Piquini, and A. Fazzio, Phys. Rev. B **67**, 113407 (2003).
[34] H. J. Xiang, J. Yang, J. G. Hou, and Q. Zhu, Phys. Rev. B **68**, 035427 (2003).
[35] S. S. Han, S. H. Lee, J. K. Kang, and H. M. Lee, Phys. Rev. B **72**, 113402 (2005).
[36] M. F. Lin and Kenneth W.-K. Shung, Phys. Rev. B **50**, 17744 (1994).
[37] J. C. Slater, Phys. Rev. **36**, 57 (1930).
[38] Kenneth W.-K. Shung, Phys. Rev. B **34**, 979 (1986).
[39] S. L. Adler, Phys. Rev. **126**, 413 (1962); N. Wiser, *ibid.* **129**, 62 (1963).
[40] W. Hanke and L. J. Sham, Phys. Rev. B **12**, 4501 (1975).
[41] G. Y. Guo, S. Ishibashi, T. Tamura, and K. Terakura, Phys. Rev. B **75**, 245403 (2007).
[42] L. D. Landau, E. M. Lifshitz, and L. P. Pitaevskii, *Electrodynamics of Continuous Media*, 2nd ed. (Pergamon, Oxford, 1984).
[43] The above discussion possibly sheds some light on the origin of several nondispersive low-energy peaks (below 3.5 eV) observed in the momentum-dependent EELS measurements performed on bulk samples of single-walled CNTs [see T. Pichler, M. Knupfer, M. S. Golden, J. Fink, A. Rinzler, and R. E. Smalley, Phys. Rev. Lett. **80**, 4729 (1998); M. Knupfer, T. Pichler, M. S. Golden, J. Fink, A. Rinzler, and R. E. Smalley, Carbon **37**, 733 (1999)]. Although there has been a number of attempts to give a theoretical explanation of these features, briefly summarized in Ref. 24, there is still no consensus regarding their true origin. One cannot exclude that these features correspond to the solutions of Eq. (46), which may differ from the zeros of the real part of $\varepsilon_L(\omega,q)$. In this case, the low-energy resonant structures observed by Pichler *et al.* may be associated neither with collective modes nor with excitations between delocalized and localized electronic states, as was initially assumed by Pichler *et al.* Note that one way to see that the above-mentioned solutions of Eq. (46) are not collective modes is to use Eq. (44) to show that the corresponding $\Gamma_L(q)$ is negative.